Supplement of

Southern African dust aerosols are rich in micronutrients, K-feldspar and carbonate minerals

Clarissa Baldo et al.

Correspondence to: Clarissa Baldo (clarissa.baldo@lisa.ipsl.fr)

List of Abbreviations

AMMA = African Monsoon Multidisciplinary Analysis (2006), special observation period 0 (SOP0), Niger (Rajot et al., 2008); special observation periods 1 and 2 (SOP1-2), West Africa (Reeves et al., 2010).

DABEX = Dust And Biomass-burning Experiment (2006), Niger (Haywood et al., 2008)

DODO = Dust Outflow and Deposition to the Oceans (2006), Senegal (McConnell et al., 2008)

FENNEC = The Saharan Climate System (2010−2012), West Africa (Washington et al., 2012)

GERBILS = Geostationary Earth Radiation Budget Intercomparisons of Longwave and Short−wave radiation (2007), Mauritania, Mali, and Niger (Haywood et al., 2011)

CESAM = Multiphase Atmospheric Experimental Simulation Chamber (Wang et al., 2011)

GAMEL = Générateur d'Aérosol Minéral En Laboratoire (Lafon et al., 2014)

Aus = Australia

NAf = Northern Africa

SAf = Southern Africa

SAm = Southern America

ICP-AES = Inductively Coupled Plasma–Atomic Emission Spectroscopy

ICP-MS = Inductively Coupled Plasma–Mass Spectrometry

XRF = X-ray Fluorescence

XRD = X-ray Diffraction

PIXE = Particle-Induced X-ray Emission

PIGE = Particle-Induced Gamma-ray Emission

SEM = Scanning Electron Microscopy

PM_{10} = Particles with an aerodynamic diameter less than 10 μm

$PM_{2.6}$ = Particles with an aerodynamic diameter less than 2.6 μm

PM_{9} = Particles with an aerodynamic diameter less than 9 μm

TSP = Total Suspended Particles

Table S1. Summary of dust aerosol samples and analyses in this study. For the sample collected along riverbed transects at ~100 m intervals, the reported coordinate represents an approximate central location of the transect.

Sample ID	Location	Latitude	Longitude	Generation	Available analyses
Kuiseb	Kuiseb River	-23.135	14.57395	GAMEL	XRF, XRD
Hope-Mine	Hope Mine	-23.5713	15.25013	GAMEL	XRF, XRD
GB-WF	Namib GP	-23.4509	15.03569	GAMEL	XRF, XRD
Etosha-West	Etosha Pan	-19.1249	15.97	GAMEL	XRF, XRD
233-TRP	Skukuza	-24.9948	31.5887	GAMEL	XRF, XRD
232-TRP	Skukuza	-24.9948	31.5887	GAMEL	XRF, XRD
199-KAL	Kalahari BOT	-26.8248	20.67703	GAMEL	XRF, XRD
184-BSW	Kalahari BOT	-18.3642	21.84194	GAMEL	XRF, XRD
179-BSW	Kalahari BOT	-20.9767	22.48	GAMEL	XRF, XRD
MS-AGR	Free State	-28.21	26.15	GAMEL	XRF, XRD
HUAB_H123	Huab River transect	-20.86	13.65	CESAM	XRF
HUAB_H125	Huab River transect	-20.86	13.65	CESAM	XRF
HUAB_H127B	Huab River transect	-20.86	13.65	CESAM	XRF
HUAB_H127A	Huab River transect	-20.86	13.65	CESAM	XRF, XRD
HUAB_H129	Huab River transect	-20.86	13.65	CESAM	XRF, XRD
HUAB_H130	Huab River transect	-20.86	13.65	CESAM	XRF
HUAB_H131	Huab River transect	-20.86	13.65	CESAM	XRF, XRD
HUAB_H132	Huab River transect	-20.86	13.65	CESAM	XRF
HUAB_H133	Huab River transect	-20.86	13.65	CESAM	XRF, XRD
HUAB_H135	Huab River transect	-20.86	13.65	CESAM	XRF, XRD
HUAB_H139	Huab River transect	-20.86	13.65	CESAM	XRF
HUAB_H141	Huab River transect	-20.86	13.65	CESAM	XRF
HUAB_H143	Huab River transect	-20.86	13.65	CESAM	XRF
K89_AERO	Kuiseb River transect	-23.18	14.65	CESAM	XRF
K99_AERO	Kuiseb River transect	-23.18	14.65	CESAM	XRF
K103_AERO	Kuiseb River transect	-23.18	14.65	CESAM	XRF
K105_AERO	Kuiseb River transect	-23.18	14.65	CESAM	XRF
K109_AERO	Kuiseb River transect	-23.18	14.65	CESAM	XRF
K111_AERO	Kuiseb River transect	-23.18	14.65	CESAM	XRF
K113_AERO	Kuiseb River transect	-23.18	14.65	CESAM	XRF
K115_AERO	Kuiseb River transect	-23.18	14.65	CESAM	XRF
OMANN_O40	Omaruru River transect	-22.03	14.35	CESAM	XRF
OMANN_O44	Omaruru River transect	-22.03	14.35	CESAM	XRF
O46_AERO	Omaruru River transect	-22.03	14.35	CESAM	XRF
OMANN_O46	Omaruru River transect	-22.03	14.35	CESAM	XRF
OMANN_O51	Omaruru River transect	-22.03	14.35	CESAM	XRF
O51_AERO	Omaruru River transect	-22.03	14.35	CESAM	XRF

OMANN_O65	Omaruru River transect	-22.03	14.35	CESAM	XRF
OMANN_O67	Omaruru River transect	-22.03	14.35	CESAM	XRF
O67_AERO	Omaruru River transect	-22.03	14.35	CESAM	XRF
OMANN_O69	Omaruru River transect	-22.03	14.35	CESAM	XRF
OMANN_O71	Omaruru River transect	-22.03	14.35	CESAM	XRF
OMANN_O73	Omaruru River transect	-22.03	14.35	CESAM	XRF
OMANN_O75	Omaruru River transect	-22.03	14.35	CESAM	XRF

Table S2. Summary of data sources included in the integrated dataset of elemental composition and mineralogy of mineral dust.

Region	Reference	Study Area	Aerosol Collection	size	Data Type	Analytical technique
SAf	This study	Central Namib Gravel Plain; Western Kalahari; Etosha Pan, Huab, Omaruru, and Kuiseb riverbeds; savannah soils in South Africa; agricultural soils in the Free State; mining dust from Namibia	Laboratory soil-derived	PM_{10}	Elemental composition, Mineralogy	XRF; XRD
	Di Biagio et al. (2017)	Central Namib Gravel Plain	Laboratory soil-derived	PM_{10}	Elemental composition, Mineralogy	XRF; XRD
	Eltayeb et al. (1993)	Central Namib Gravel Plain	Laboratory soil-derived	$PM_{2.6}$	Elemental composition	XRF
	Engelbrecht et al. (2016)	Etosha Pan; Makgadikgadi Pans; Nxai Pan	Laboratory soil-derived	PM_{10}	Elemental composition	XRF
	Humphries et al. (2014)	Okavango Delta	Ground-based, near source	TSP	Elemental composition	XRF
	Qu (2016)	Central Namib Gravel Plain; Western Kalahari	Laboratory soil-derived	PM_{10}	Elemental composition	XRF
Aus	Box et al. (Jan 27-29 2010)	Lake Eyre Basin	Ground-based, transported	TSP	Elemental composition	PIXE and PIGE
	Di Biagio et al. (2017)	Lake Eyre Basin	Laboratory soil-derived	PM_{10}	Elemental composition, Mineralogy	XRF; XRD
	Engelbrecht et al. (2016)	Lake Eyre Basin	Laboratory soil-derived	PM_{10}	Elemental composition	XRF
	Moreno et al. (2008)	Lake Eyre Basin	Laboratory soil-derived	PM_{10}	Elemental composition	ICP-AES; ICP-MS
	Radhi et al. (2010a, 2010b)	Lake Eyre Basin	Ground-based, near source	TSP	Elemental composition	PIXE and PIGE
	Karlson et al. (2014)	Lake Eyre Basin; Northwestern Australia	Ground-based, near source and transported	TSP	Elemental composition	PIXE and PIGE
SAm	Demasy et al. (2024)	Patagonia	Laboratory soil-derived	PM_{10}	Elemental composition	ICP-MS
	Di Biagio et al. (2017)	Patagonia; Atacama Desert	Laboratory soil-derived	PM_{10}	Elemental composition, Mineralogy	XRF; XRD
	Engelbrecht et al. (2016)	Atacama Desert	Laboratory soil-derived	PM_{10}	Elemental composition	XRF
	Gaiero et al. (2007); (2003)	Patagonia	Ground-based, transported	TSP	Elemental composition	ICP-AES; ICP-MS
	Qu (2016)	Patagonia	Laboratory soil-derived	PM_{10}	Elemental composition	XRF

	Rojas et al. (1990)	Atacama Desert; Remote sites across Argentina, Bolivia, and Brazil	Ground-based, near source	TSP	Elemental composition	XRF
NAf	Di Biagio et al. (2017)	Sahara Desert; Sahel; Bodélé Depression	Laboratory soil-derived	PM_{10}	Elemental composition, Mineralogy	XRF; XRD
	Engelbrecht et al. (2016)	Sahel; Bodélé Depression; Lake Iriki	Laboratory soil-derived	PM_{10}	Elemental composition	XRF
	Formenti et al. (2014)	West Africa (AMMA-SOP-1/2); Niger (AMMA-SOP0; DABEX); Senegal (DODO); Mauritania, Mali, Niger (GERBLIS)	Aircraft, near source; Ground-based, near source	$PM_{9;}$ PM_{10}	Elemental composition, Mineralogy	PIXE; XRD
	Formenti et al. (2011)	West Africa (AMMA-SOP-1)	Ground-based, near source	PM_9	Elemental composition	XRF
	Formenti et al. (2008)	Niger (AMMA-SOP0, DABEX); Senegal (DODO)	Aircraft, near source; Ground-based, near source	PM_{10}	Elemental composition, Mineralogy	PIXE; XRD
	Klaver et al. (2011)	Mauritania, Mali, Niger (GERBLIS)	Aircraft, near source	PM_{10}	Elemental composition, Mineralogy	PIXE; XRD
	(Ryder et al., 2015)	West Africa (FENNEC)	Aircraft, near source	PM_{10}	Elemental composition	SEM

Table S3. Location and references to the integrated dataset on SAf dust chemical tracers. Atmospheric observations are included for comparison.

Location ID	Description	References
Namib GP	Central Namib Gravel Plain, western Namibia.	This study; Di Biagio et al. (2017); Qu (2016)
Kalahari NAM	Western Kalahari, central Namibia	Qu (2016)
Kalahari BOT	Southwestern Kalahari, southwestern Botswana. Areas of the Kalahari north and south of the Okavango Delta, northwestern Botswana	This study
Salt Pans	Etosha Pan, northern Namibia. Makgadikgadi and Nxai Pans, northeastern Botswana	This study (Etosha Pan only); (Engelbrecht et al., 2016).
Coastal rivers	Ephemeral riverbeds on the Namibian coast, including Huab, Omaruru, and Kuiseb rivers	This Study
Skukuza	Savannah soils at Skukuza in the Kruger National Park, South Africa	This Study
Hope Mine	Abandoned copper mine, central western Namibia	This Study
Free State	Agricultural soils in the Free State	This Study
Henties Bay – Dust mixed aerosols	Atmospheric aerosols over the Namibian coast	Desboeufs et al. (2024); Formenti et al. (2025); Klopper et al. (2020)
SA Highveld – Dust mixed aerosols	Atmospheric aerosols over the South African Highveld, an inland urban-industrial environment	Baldo et al. (2025)

Table S4. Summary statistics of elemental enrichment factors in mineral dust across Southern Africa, Australia, Southern America, and Northern Africa. Data source references are provided in Table S2.

Region	Element	N total	Mean	Median	sd	25th percentile	75th percentile	Min	Max
SAf	Si	72	1.39	0.74	2.64	0.67	1.00	0.45	18.36
	Mg	70	7.20	1.98	18.45	1.16	4.71	0.31	109.52
	K	70	1.80	1.17	1.99	1.06	1.78	0.00	12.49
	Ca	72	7.02	1.27	16.13	0.82	4.61	0.00	96.39
	Fe	72	1.69	1.62	0.92	1.20	1.71	0.93	7.03
	Mn	63	2.82	1.88	3.67	0.95	3.13	0.00	18.33
	P	63	2.55	1.70	1.87	1.11	3.34	0.64	7.34
	Na	63	0.62	0.35	2.06	0.17	0.57	0.00	16.55
	Ti	70	2.11	1.54	1.20	1.37	2.89	0.00	6.16
Aus	Si	49	1.25	0.82	1.85	0.67	0.97	0.37	12.54
	Mg	12	0.62	0.53	0.40	0.36	0.64	0.28	1.74
	K	16	0.75	0.82	0.41	0.38	0.92	0.23	1.75
	Ca	21	0.56	0.46	0.52	0.30	0.63	0.09	2.38
	Fe	57	1.87	1.75	0.75	1.35	2.24	0.52	4.74
	Mn	49	2.73	1.66	2.98	1.16	3.16	0.12	18.22
	P	9	0.89	0.83	0.21	0.77	0.98	0.60	1.28
	Na	13	0.37	0.12	0.63	0.05	0.19	0.03	2.25
	Ti	52	1.59	1.19	1.02	0.82	2.33	0.32	4.09
NAf	Si	508	0.65	0.64	0.12	0.60	0.70	0.15	1.49
	Mg	508	0.70	0.63	0.39	0.42	0.88	0.00	2.63
	K	508	0.60	0.60	0.27	0.46	0.71	0.00	1.88
	Ca	508	1.00	0.75	1.37	0.28	1.30	0.00	18.87
	Fe	508	1.25	1.24	0.33	1.15	1.35	0.00	4.72
	Mn	10	2.40	1.72	1.69	1.57	2.53	0.96	6.46
	P	501	1.20	1.23	0.61	1.00	1.47	0.00	6.64
	Na	501	0.16	0.02	0.49	0.00	0.16	0.00	8.89
	Ti	508	1.95	1.92	0.81	1.62	2.24	0.00	9.26
SAm	Si	160	1.05	1.00	0.25	0.91	1.22	0.29	2.11
	Mg	152	1.54	1.30	1.01	0.94	2.14	0.00	5.76
	K	152	1.37	1.37	0.44	1.11	1.51	0.51	3.23
	Ca	160	1.89	1.44	1.75	1.07	1.91	0.15	12.43
	Fe	161	1.26	1.19	0.72	1.05	1.32	0.43	9.65
	Mn	151	2.36	1.30	3.42	0.47	2.96	0.00	26.39
	P	137	6.74	5.82	4.86	4.86	6.96	1.40	53.89

	Na	151	0.77	0.78	0.41	0.58	0.95	0.00	2.21
	Ti	152	4.12	4.06	1.59	3.44	4.89	1.06	16.57

Table S5. Summary statistics of key mineral components in mineral dust across Southern Africa, Australia, Southern America, and Northern Africa. Data source references are provided in Table S2.

Region	Mineral	N total	Mean	Median	sd	25th percentile	75th percentile	Min	Max
SAf	Quartz	18	13	10	10	7	14	0	37
	Clays	18	62	61	14	57	70	21	87
	Carbonates	18	8	4	18	0	4	0	78
	Feldspars	18	15	16	13	2	26	0	34
Aus	Quartz	1	34	34	-	34	34	34	34
	Clays	1	57	57	-	57	57	57	57
	Carbonates	1	0	0	-	0	0	0	0
	Feldspars	1	6	6	-	6	6	6	6
NAf	Quartz	61	12	10	8	7	13	1	41
	Clays	61	84	87	11	84	91	49	96
	Carbonates	61	2	1	5	0	2	0	26
	Feldspars	61	1	1	2	0	1	0	14
SAm	Quartz	2	26	26	22	18	34	11	42
	Clays	2	60	60	13	56	65	51	69
	Carbonates	2	6	6	9	3	9	0	12
	Feldspars	2	6	6	0	6	6	6	6

Text S1. Data processing of aerosol size distribution measurements.

The experiments conducted with GAMEL and CESAM employ different generation methods and instrumentation setups, necessitating distinct data-processing approaches.

For GAMEL experiments, the size-distribution data were converted into volume distributions ($\pi/6 \cdot D^3 \cdot dN/dlogD$), where D is the particle diameter measured by the instrument. To allow comparison between samples while accounting for differences in dust-generation efficiency among soils, data were retained only for the first 3 minutes of dust generation, normalised so that the integral equals 1 over a common diameter range (the full diameter range measured by the GRIMM), and averaged. Repeated experiments on the same soil samples under the same shaking conditions were averaged.

For the CESAM experiments, the protocol for data reduction to obtain the aerosol dust size distribution is established as part of the CESAM procedures and is described in detail elsewhere (Di Biagio et al., 2019; Di Biagio et al., 2017). The first step of the procedure converts the working diameters of the SMPS, GRIMM, and WELAS instruments (which are, respectively, electrical mobility and optical diameters) into a sphere-equivalent geometric diameter (D_g). Di Biagio et al. (2019) have shown that the correction factor for the optical particle counters (OPCs, WELAS and GRIMM) is less sensitive to the complex refractive index in the range of values expected for mineral dust in the visible and near-infrared. In this study, we assume an average refractive index of 1.53 + 0.004i for both the WELAS and the GRIMM, yielding estimated Dg values of 0.65-73.0 µm for the WELAS and 0.29-68.2 µm for the GRIMM. The average dry aerodynamic shape factor required to convert the electrical mobility diameter measured by the SMPS to geometric diameter is 1.2, which best matches the SMPS number size distribution with those of the GRIMM or WELAS in their overlap range. The aerosol dust number size distribution between 10 nm and 73 µm can then be obtained by combining the number size distributions measured by the different probes. For these experiments, the GRIMM is preferred over the WELAS for particles smaller than approximately 800 nm due to its higher counting efficiency. Due to size-dependent particle losses in the sampling lines, the measured number size distributions are reduced in size range from 0.01 to 23.7 µm, which is consistent with previous work (Baldo et al., 2023; Caponi et al., 2017; Di Biagio et al., 2019). For comparison with GAMEL, only measurements collected shortly after the dust injection peak in CESAM were retained, as larger particles are rapidly lost by gravitational settling. The data were converted to volume distributions, normalised so that the integral equals 1 over a common diameter range, averaged, and interpolated using the "smooth.spline" function from the core CRAN R software to obtain values over a consistent diameter range, matching the GAMEL experimental data.

Text S2. Data source for the rainfall map of Southern Africa

The rainfall map of Southern Africa is derived from the Climate Hazard Group InfraRed Precipitation with Stations dataset version 3 (CHIRPS3, 2025). This dataset integrates satellite-based thermal infrared rainfall estimates with ground-based observations, at a spatial resolution of 0.05° by 0.05°, covering the global domain and including additional sub-domain datasets. It contains long-term rainfall records from 1981 to the near present, with temporal resolutions ranging from daily to annual. For our analysis, we used ten years of annual rainfall data for the Africa sub-domain product from 2015 to 2024.

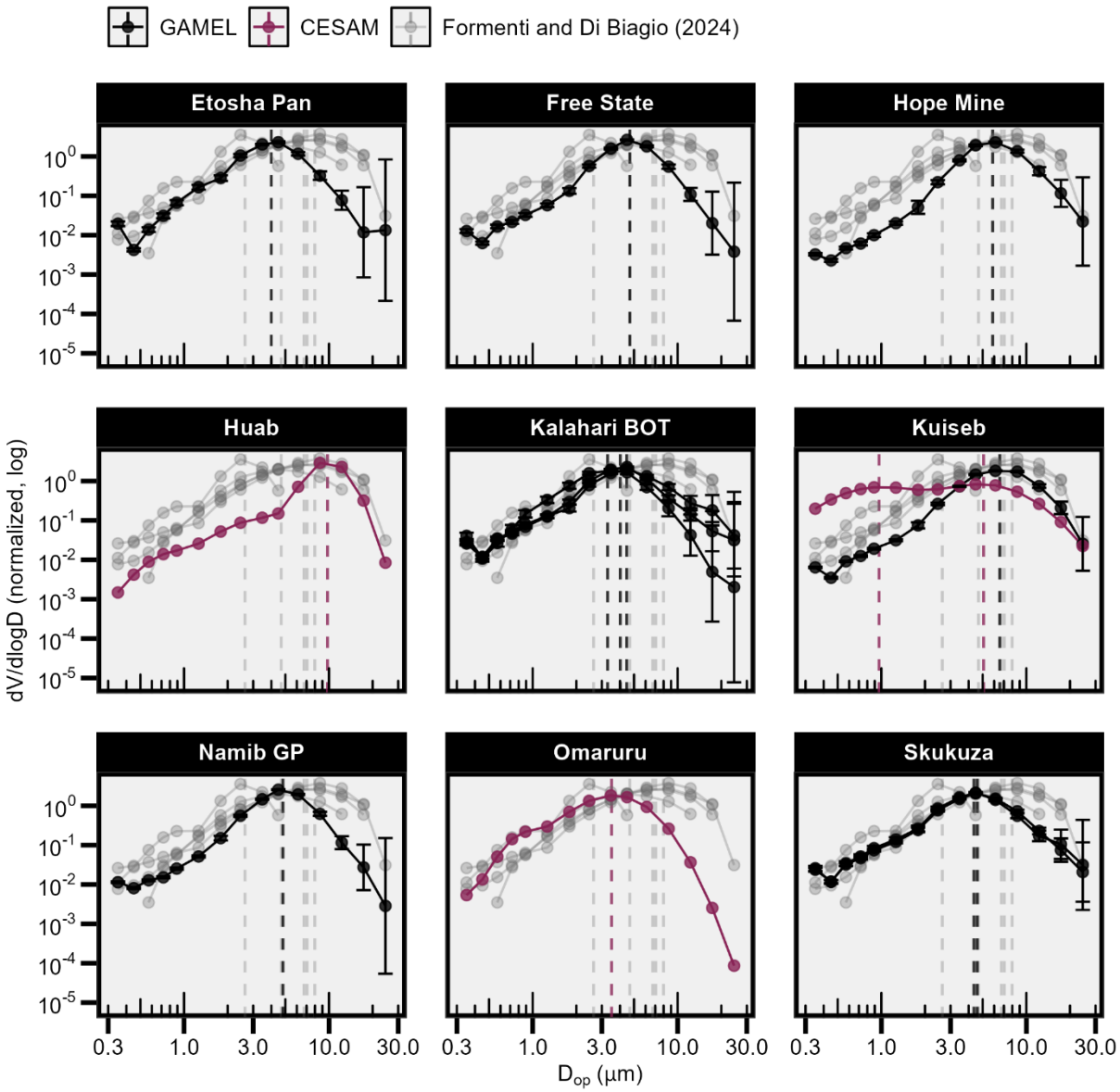

Figure S1. Size distribution data obtained during the laboratory generation of dust aerosols using GAMEL aerosol generator and the CESAM multiphase simulation chambers. Observations of PM_{10} and PM_{20} aerosols collected near source regions from the integrated dataset compiled by Formenti and Di Biagio (2024) (including Fratini et al., 2007; Gillette et al., 1974; Rajot et al., 2008; Shao et al., 2011; Sow et al., 2009) are shown for comparison. Data are reported as volume distributions ($\mu m^3\ cm^{-3}$) normalised so that the integral equals 1 over a common diameter range. The dashed lines indicate the peaks of the single-mode log-normal fitted distributions. Only the aerosol sample generated in CESAM from Kuiseb River sediments exhibits an additional peak at 1 µm.

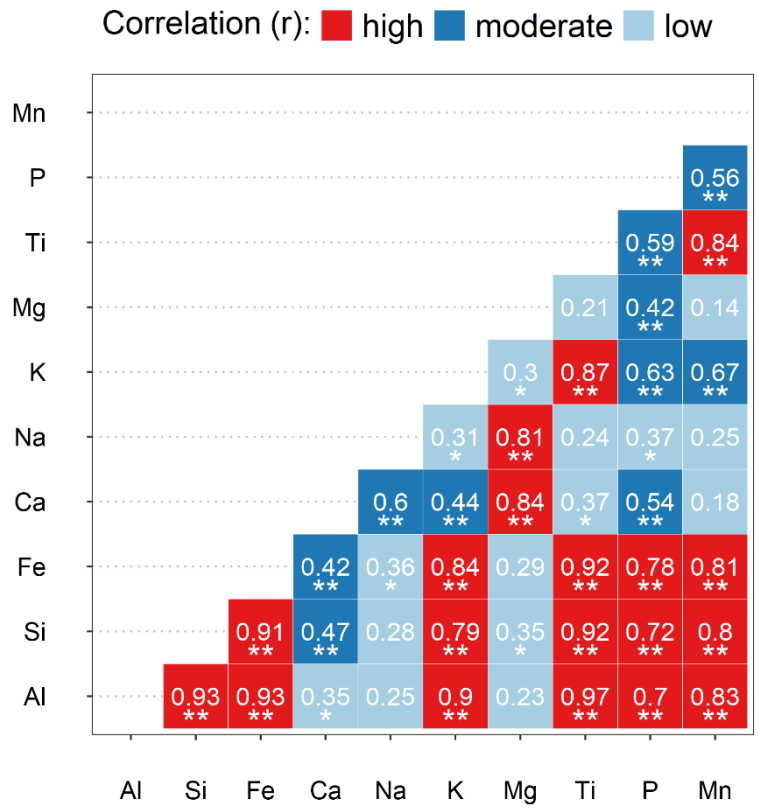

Figure S2. Correlations between crustal elements. The correlation matrix reports estimated r values from linear regression. Note that * indicates p-values ≤ 0.05, while ** indicates p-values ≤ 0.01.

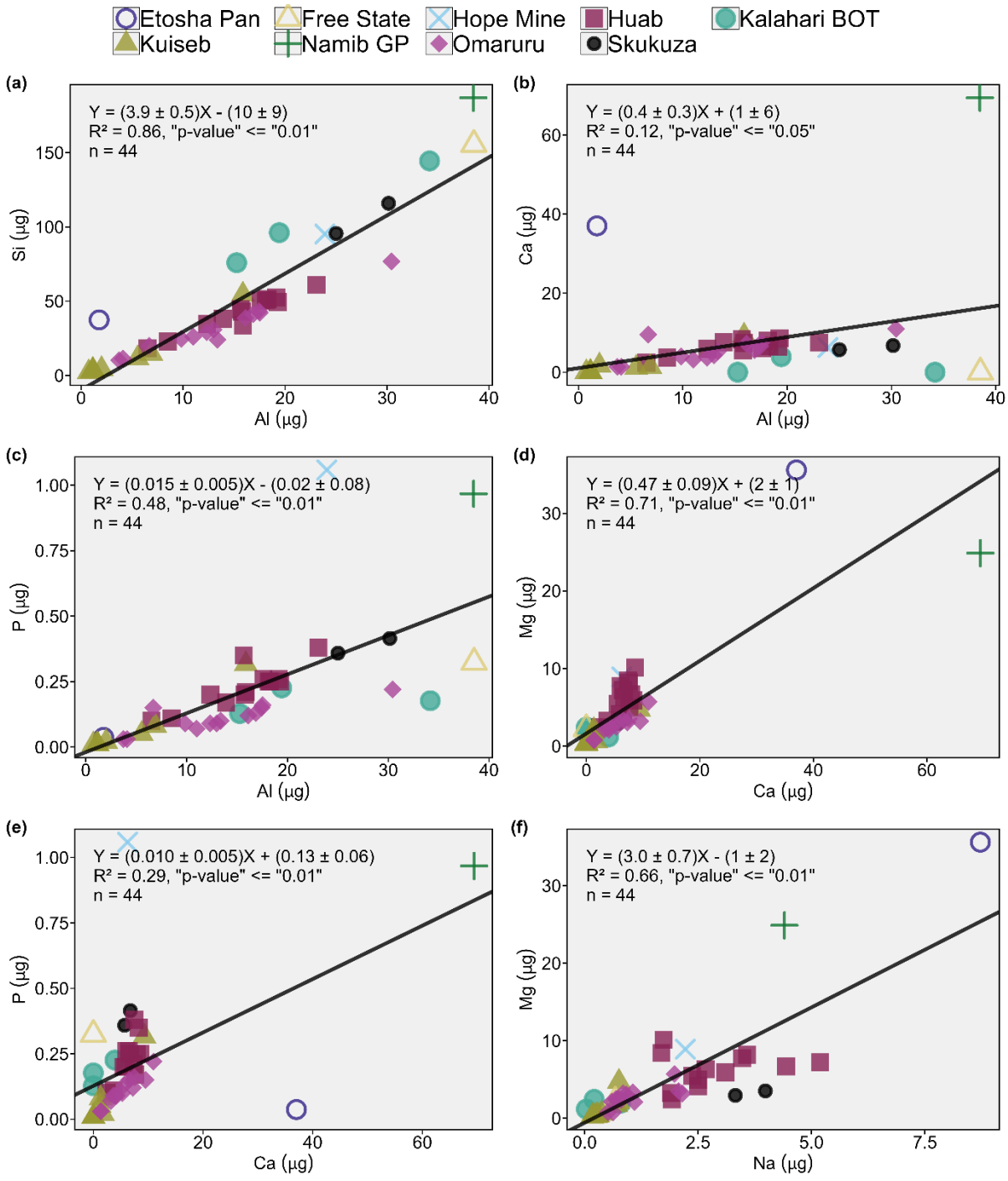

Figure S3. Key element correlations supporting the correlation matrix in Figure S2. The analysis includes all data points. Uncertainty in XRF measurements is 10%.

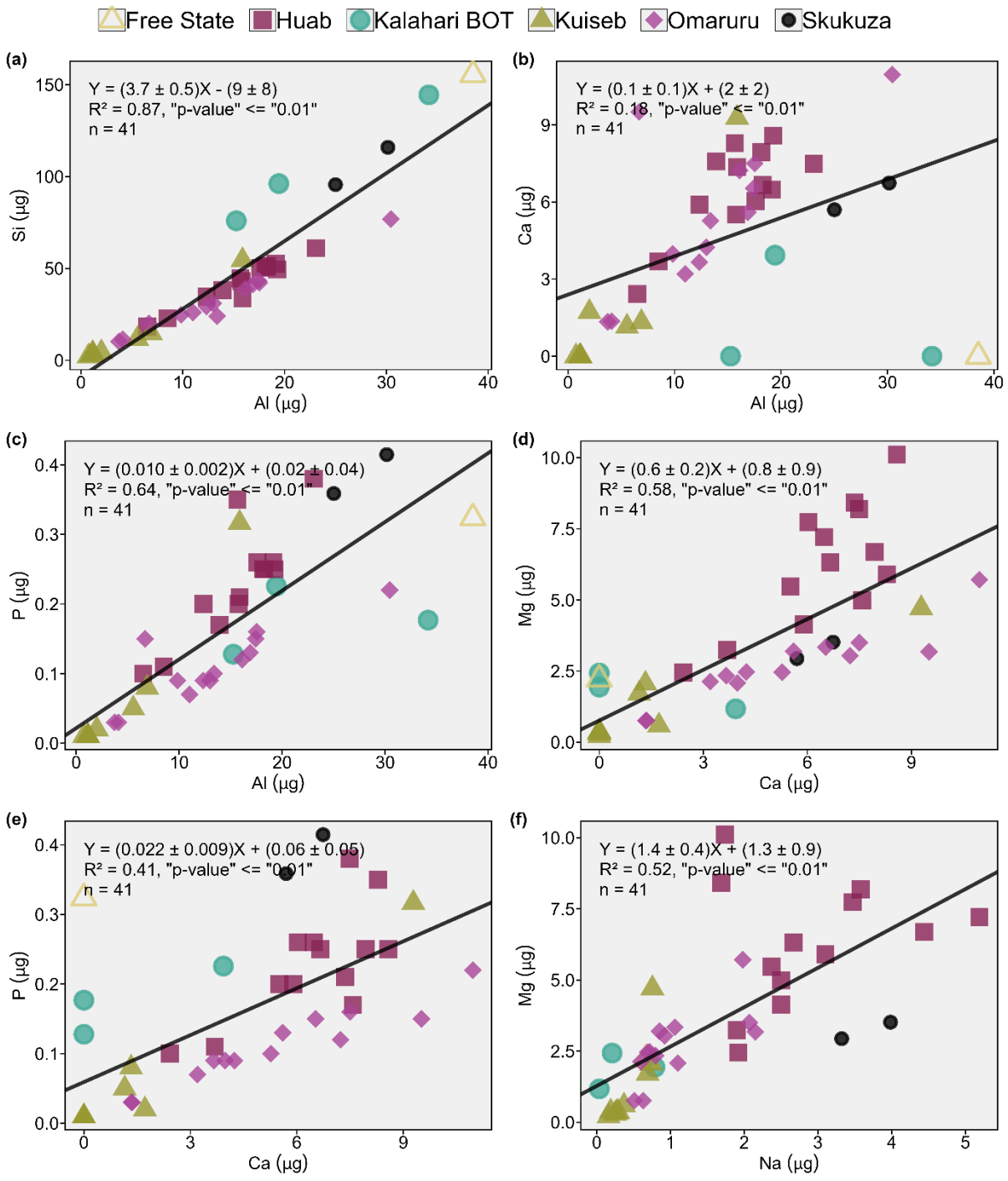

Figure S4. Key element correlations supporting the correlation matrix in Figure S2. Namib GB, Etosha Pan, and Hope Mine are not included. Key correlations are maintained even after removing extreme values. Uncertainty in XRF measurements is 10%.

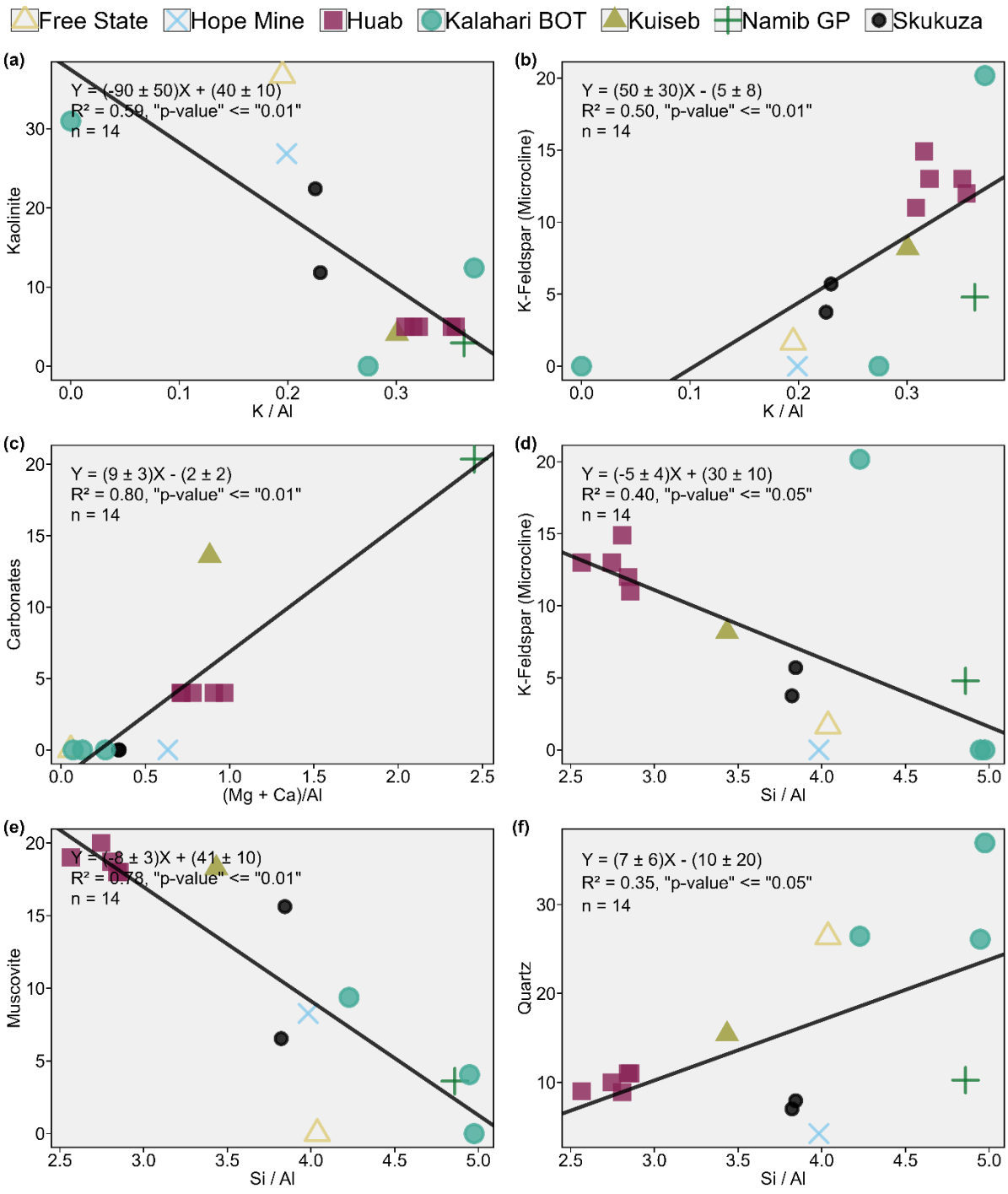

Figure S5. Correlations between key crustal element ratios and minerals. Note that Etosha Pan was excluded from the analysis because its composition significantly differs from the other dust samples. Uncertainty in XRF and XRD measurements is 10%.

References

Baldo, C., Formenti, P., Di Biagio, C., Lu, G., Song, C., Cazaunau, M., Pangui, E., Doussin, J. F., Dagsson-Waldhauserova, P., Arnalds, O., Beddows, D., MacKenzie, A. R., and Shi, Z.: Complex refractive index and single scattering albedo of Icelandic dust in the shortwave part of the spectrum, Atmospheric Chemistry and Physics, 23, 7975-8000, doi: 10.5194/acp-23-7975-2023, 2023.

Baldo, C., Language, B., Isolabella, T., Vernocchi, V., Massabò, D., van Zyl, P. G., Annegarn, H. J., Piketh, S., and Formenti, P.: Low-Level Urban Anthropogenic Sources Contribute to Strong Aerosol Light Absorption on the South African Highveld, Journal of Geophysical Research-Atmospheres, 130, e2024JD042846, doi: 10.1029/2024jd042846, 2025.

Box, M. A., Radhi, M., and Box, G. P.: The great Sydney dust event: size-resolved chemical composition and comparison, in: IOP Conference Series-Earth and Environmental Science, 17th National Conference of the Australian Meteorological and Oceanographic Society, Canberra, AUSTRALIA, Jan 27-29 2010, doi: 10.1088/1755-1315/11/1/012015, 2010.

Caponi, L., Formenti, P., Massabo, D., Di Biagio, C., Cazaunau, M., Pangui, E., Chevaillier, S., Landrot, G., Andreae, M. O., Kandler, K., Piketh, S., Saeed, T., Seibert, D., Williams, E., Balkanski, Y., Prati, P., and Doussin, J. F.: Spectral- and size-resolved mass absorption efficiency of mineral dust aerosols in the shortwave spectrum: a simulation chamber study, Atmospheric Chemistry and Physics, 17, 7175-7191, doi: 10.5194/acp-17-7175-2017, 2017.

CHIRPS3: Climate Hazards Center Infrared Precipitation with Stations version 3. CHIRPS3 Data Repository https://doi.org/10.15780/G2JQ0P (2025). Data was accessed on [August 2025], in, 2025.

Demasy, C., Boye, M., Lai, B., Burckel, P., Feng, Y., Losno, R., Borensztajn, S., and Besson, P.: Iron dissolution from Patagonian dust in the Southern Ocean: under present and future conditions, Frontiers in Marine Science, 11, 1363088, doi: 10.3389/fmars.2024.1363088, 2024.

Desboeufs, K., Formenti, P., Torres-Sánchez, R., Schepanski, K., Chaboureau, J. P., Andersen, H., Cermak, J., Feuerstein, S., Laurent, B., Klopper, D., Namwoonde, A., Cazaunau, M., Chevaillier, S., Feron, A., Mirande-Bret, C., Triquet, S., and Piketh, S.: Fractional solubility of iron in mineral dust aerosols over coastal Namibia: a link to marine biogenic emissions?, Atmospheric Chemistry and Physics, 24, 1525-1541, doi: 10.5194/acp-24-1525-2024, 2024.

Di Biagio, C., Formenti, P., Balkanski, Y., Caponi, L., Cazaunau, M., Pangui, E., Journet, E., Nowak, S., Caquineau, S., Andreae, M. O., Kandler, K., Saeed, T., Piketh, S., Seibert, D., Williams, E., and Doussin, J. F.: Global scale variability of the mineral dust long-wave refractive index: a new dataset of in situ measurements for climate modeling and remote sensing, Atmospheric Chemistry and Physics, 17, 1901-1929, doi: 10.5194/acp-17-1901-2017, 2017.

Di Biagio, C., Formenti, P., Balkanski, Y., Caponi, L., Cazaunau, M., Pangui, E., Journet, E., Nowak, S., Andreae, M. O., Kandler, K., Saeed, T., Piketh, S., Seibert, D., Williams, E., and Doussin, J. F.: Complex refractive indices and single-scattering albedo of global dust aerosols in the shortwave spectrum and relationship to size and iron content, Atmospheric Chemistry and Physics, 19, 15503-15531, doi: 10.5194/acp-19-15503-2019, 2019.

Eltayeb, M. A. H., Vangrieken, R. E., Maenhaut, W., and Annegarn, H. J.: AEROSOL SOIL FRACTIONATION FOR NAMIB DESERT SAMPLES, Atmospheric Environment Part a-General Topics, 27, 669-678, doi: 10.1016/0960-1686(93)90185-2, 1993.

Engelbrecht, J. P., Moosmuller, H., Pincock, S., Jayanty, R. K. M., Lersch, T., and Casuccio, G.: Technical note: Mineralogical, chemical, morphological, and optical interrelationships of mineral dust re-suspensions, Atmospheric Chemistry and Physics, 16, 10809-10830, doi: 10.5194/acp-16-10809-2016, 2016.

Formenti, P., Rajot, J. L., Desboeufs, K., Caquineau, S., Chevaillier, S., Nava, S., Gaudichet, A., Journet, E., Triquet, S., Alfaro, S., Chiari, M., Haywood, J., Coe, H., and Highwood, E.: Regional variability of the composition of mineral dust from western Africa: Results from the AMMA SOP0/DABEX and DODO field campaigns, Journal of Geophysical Research-Atmospheres, 113, doi: 10.1029/2008jd009903, 2008.

Formenti, P., Rajot, J. L., Desboeufs, K., Saïd, F., Grand, N., Chevaillier, S., and Schmechtig, C.: Airborne observations of mineral dust over western Africa in the summer Monsoon season: spatial and vertical variability of physico-chemical and optical properties, Atmos. Chem. Phys., 11, 6387-6410, doi: 10.5194/acp-11-6387-2011, 2011.

Formenti, P., Caquineau, S., Desboeufs, K., Klaver, A., Chevaillier, S., Journet, E., and Rajot, J. L.: Mapping the physico-chemical properties of mineral dust in western Africa: mineralogical composition, Atmospheric Chemistry and Physics, 14, 10663-10686, doi: 10.5194/acp-14-10663-2014, 2014.

Formenti, P., and Di Biagio, C.: Large synthesis of in situ field measurements of the size distribution of mineral dust aerosols across their life cycles, Earth System Science Data, 16, 4995-5007, doi: 10.5194/essd-16-4995-2024, 2024.

Formenti, P., Giorio, C., Desboeufs, K., Zherebker, A., Gaetani, M., Baldo, C., Landrot, G., Montebello, S., Chevaillier, S., Triquet, S., Siour, G., Di Biagio, C., Battaglia, F., Doussin, J. F., Feron, A., Namwoonde, A., and Piketh, S. J.: Elemental composition, iron mineralogy and solubility of anthropogenic and natural mineral dust aerosols in Namibia: a case study analysis from the AEROCLO-sA campaign, EGUsphere, 2025, 1-28, doi: 10.5194/egusphere-2025-446, 2025.

Fratini, G., Ciccioli, P., Febo, A., Forgione, A., and Valentini, R.: Size-segregated fluxes of mineral dust from a desert area of northern China by eddy covariance, Atmos. Chem. Phys., 7, 2839-2854, doi: 10.5194/acp-7-2839-2007, 2007.

Gaiero, D. M., Probst, J. L., Depetris, P. J., Bidart, S. M., and Leleyter, L.: Iron and other transition metals in Patagonian riverborne and windborne materials: geochemical control and transport to the southern South Atlantic Ocean, Geochimica Et Cosmochimica Acta, 67, 3603-3623, doi: 10.1016/S0016-7037(03)00211-4, 2003.

Gaiero, D. M., Brunet, F., Probst, J.-L., and Depetris, P. J.: A uniform isotopic and chemical signature of dust exported from Patagonia: Rock sources and occurrence in southern environments, Chemical Geology, 238, 107-120, doi: 10.1016/j.chemgeo.2006.11.003, 2007.

Gillette, D. A., Blifford Jr., I. H., and Fryrear, D. W.: The influence of wind velocity on the size distributions of aerosols generated by the wind erosion of soils, Journal of Geophysical Research (1896-1977), 79, 4068-4075, doi: 10.1029/JC079i027p04068, 1974.

Haywood, J. M., Pelon, J., Formenti, P., Bharmal, N., Brooks, M., Capes, G., Chazette, P., Chou, C., Christopher, S., Coe, H., Cuesta, J., Derimian, Y., Desboeufs, K., Greed, G., Harrison, M., Heese, B., Highwood, E. J., Johnson, B., Mallet, M., Marticorena, B., Marsham, J., Milton, S., Myhre, G., Osborne, S. R., Parker, D. J., Rajot, J.-L., Schulz, M., Slingo, A., Tanré, D., and Tulet, P.: Overview of the Dust and Biomass-burning Experiment and African Monsoon Multidisciplinary Analysis Special Observing Period-0, Journal of Geophysical Research: Atmospheres, 113, doi: 10.1029/2008JD010077, 2008.

Haywood, J. M., Johnson, B. T., Osborne, S. R., Baran, A. J., Brooks, M., Milton, S. F., Mulcahy, J., Walters, D., Allan, R. P., Klaver, A., Formenti, P., Brindley, H. E., Christopher, S., and Gupta, P.: Motivation, rationale and key results from the GERBILS Saharan dust measurement campaign, Quarterly Journal of the Royal Meteorological Society, 137, 1106-1116, doi: 10.1002/qj.797, 2011.

Humphries, M. S., McCarthy, T. S., Cooper, G. R. J., Stewart, R. A., and Stewart, R. D.: The role of airborne dust in the growth of tree islands in the Okavango Delta, Botswana, Geomorphology, 206, 307-317, doi: 10.1016/j.geomorph.2013.09.035, 2014.

Karlson, L. R., Greene, R. S. B., Scott, K. M., Stelcer, E., and O'Loingsigh, T.: Characteristics of aeolian dust across northwest Australia, Aeolian Research, 12, 41-46, doi: 10.1016/j.aeolia.2013.11.003, 2014.

Klaver, A., Formenti, P., Caquineau, S., Chevaillier, S., Ausset, P., Calzolai, G., Osborne, S., Johnson, B., Harrison, M., and Dubovik, O.: Physico-chemical and optical properties of Sahelian and Saharan mineral dust: in situ measurements during the GERBILS campaign, Quarterly Journal of the Royal Meteorological Society, 137, 1193-1210, doi: 10.1002/qj.889, 2011.

Klopper, D., Formenti, P., Namwoonde, A., Cazaunau, M., Chevaillier, S., Feron, A., Gaimoz, C., Hease, P., Lahmidi, F., Mirande-Bret, C., Triquet, S., Zeng, Z. R., and Piketh, S. J.: Chemical composition and source apportionment of atmospheric aerosols on the Namibian coast, Atmospheric Chemistry and Physics, 20, 15811-15833, doi: 10.5194/acp-20-15811-2020, 2020.

Lafon, S., Alfaro, S. C., Chevaillier, S., and Rajot, J. L.: A new generator for mineral dust aerosol production from soil samples in the laboratory: GAMEL, Aeolian Research, 15, 319-334, doi: 10.1016/j.aeolia.2014.04.004, 2014.

McConnell, C. L., Highwood, E. J., Coe, H., Formenti, P., Anderson, B., Osborne, S., Nava, S., Desboeufs, K., Chen, G., and Harrison, M. A. J.: Seasonal variations of the physical and optical characteristics of Saharan dust: Results from the Dust Outflow and Deposition to the Ocean (DODO) experiment, Journal of Geophysical Research: Atmospheres, 113, D14S05, doi: 10.1029/2007JD009606, 2008.

Moreno, T., Amato, F., Querol, X., Alastuey, A., and Gibbons, W.: Trace element fractionation processes in resuspended mineral aerosols extracted from Australian continental surface materials, Australian Journal of Soil Research, 46, 128-140, doi: 10.1071/sr07121, 2008.

Qu, Z.: Chemical properties of continental aerosol transported over the Southern Ocean: Patagonian and Namibian sources. , PhD Thesis in Geochemistry. Université Pierre et Marie Curie - Paris VI, 2016., doi: https://theses.hal.science/tel-01349197v1, 2016.

Radhi, M., Box, M. A., Box, G. P., Mitchell, R. M., Cohen, D. D., Stelcer, E., and Keywood, M. D.: Optical, physical and chemical characteristics of Australian continental aerosols: results from a field experiment, Atmospheric Chemistry and Physics, 10, 5925-5942, doi: 10.5194/acp-10-5925-2010, 2010a.

Radhi, M., Box, M. A., Box, G. P., Mitchell, R. M., Cohen, D. D., Stelcer, E., and Keywood, M. D.: Size-resolved mass and chemical properties of dust aerosols from Australia's Lake Eyre Basin, Atmospheric Environment, 44, 3519-3528, doi: 10.1016/j.atmosenv.2010.06.016, 2010b.

Rajot, J. L., Formenti, P., Alfaro, S., Desboeufs, K., Chevaillier, S., Chatenet, B., Gaudichet, A., Journet, E., Marticorena, B., Triquet, S., Maman, A., Mouget, N., and Zakou, A.: AMMA dust experiment: An overview of measurements performed during the dry season special observation period (SOP0) at the Banizoumbou (Niger) supersite, Journal of Geophysical Research: Atmospheres, 113, D00C14, doi: 10.1029/2008JD009906, 2008.

Reeves, C. E., Formenti, P., Afif, C., Ancellet, G., Attié, J. L., Bechara, J., Borbon, A., Cairo, F., Coe, H., Crumeyrolle, S., Fierli, F., Flamant, C., Gomes, L., Hamburger, T., Jambert, C., Law, K. S., Mari, C., Jones, R. L., Matsuki, A., Mead, M. I., Methven, J., Mills, G. P., Minikin, A., Murphy, J. G., Nielsen, J. K., Oram, D. E., Parker, D. J., Richter, A., Schlager, H., Schwarzenboeck, A., and Thouret, V.: Chemical and aerosol characterisation of the troposphere over West Africa during the monsoon period as part of AMMA, Atmos. Chem. Phys., 10, 7575-7601, doi: 10.5194/acp-10-7575-2010, 2010.

Rojas, C. M., Figueroa, L., Janssens, K. H., Vanespen, P. E., Adams, F. C., and Vangrieken, R. E.: THE ELEMENTAL COMPOSITION OF AIRBORNE PARTICULATE MATTER IN THE ATACAMA DESERT, CHILE, Science of the Total Environment, 91, 251-267, doi: 10.1016/0048-9697(90)90302-b, 1990.

Ryder, C. L., McQuaid, J. B., Flamant, C., Rosenberg, P. D., Washington, R., Brindley, H. E., Highwood, E. J., Marsham, J. H., Parker, D. J., Todd, M. C., Banks, J. R., Brooke, J. K., Engelstaedter, S., Estelles, V., Formenti, P., Garcia-Carreras, L., Kocha, C., Marenco, F., Sodemann, H., Allen, C. J. T., Bourdon, A., Bart, M., Cavazos-Guerra, C., Chevaillier, S., Crosier, J., Darbyshire, E., Dean, A. R., Dorsey, J. R., Kent, J., O'Sullivan, D., Schepanski, K., Szpek, K., Trembath, J., and Woolley, A.: Advances in understanding mineral dust and boundary layer processes over the Sahara from Fennec aircraft observations, Atmos. Chem. Phys., 15, 8479-8520, doi: 10.5194/acp-15-8479-2015, 2015.

Shao, Y., Ishizuka, M., Mikami, M., and Leys, J. F.: Parameterization of size-resolved dust emission and validation with measurements, Journal of Geophysical Research: Atmospheres, 116, D08203, doi: 10.1029/2010JD014527, 2011.

Sow, M., Alfaro, S. C., Rajot, J. L., and Marticorena, B.: Size resolved dust emission fluxes measured in Niger during 3 dust storms of the AMMA experiment, Atmos. Chem. Phys., 9, 3881-3891, doi: 10.5194/acp-9-3881-2009, 2009.

Wang, J., Doussin, J. F., Perrier, S., Perraudin, E., Katrib, Y., Pangui, E., and Picquet-Varrault, B.: Design of a new multi-phase experimental simulation chamber for atmospheric photosmog, aerosol and cloud chemistry research, Atmospheric Measurement Techniques, 4, 2465-2494, doi: 10.5194/amt-4-2465-2011, 2011.

Washington, R., Flamant, C., Parker, D., Marsham, J., McQuaid, J., Brindley, H., Todd, M., Highwood, E., Ryder, C., and Chaboureau, J.: Fennec–the Saharan climate system, CLIVAR Exchanges, 17, 31-33, 2012.